

Self-consistent pseudopotential calculation of the bulk properties of Mo and W

Alex Zunger* and Marvin L. Cohen

Department of Physics, University of California and Materials and Molecular Research Division,
Lawrence Berkeley Laboratory, Berkeley, California 94720

(Received 7 August 1978)

The bulk properties of Mo and W are calculated using the recently developed momentum-space approach for calculating total energy via a nonlocal pseudopotential. This approach avoids any shape approximation to the variational charge density (e.g., muffin tins), is fully self-consistent, and replaces the multidimensional and multicenter integrals akin to real-space representations by simple and readily convergent reciprocal-space lattice sums. We use first-principles atomic pseudopotentials which have been previously demonstrated to yield band structures and charge densities for both semiconductors and transition metals in good agreement with experiment and all-electron calculations. Using a mixed-basis representation for the crystalline wave function, we are able to accurately reproduce both the localized and itinerant features of the electronic states in these systems. These first-principles pseudopotentials, together with the self-consistent density-functional representation for both the exchange and the correlation screening, yields agreement with experiment of 0.2% in the lattice parameters, 2% and 11% for the binding energies of Mo and W, respectively, and 12% and 7% for the bulk moduli of Mo and W, respectively.

I. INTRODUCTION

Recently,^{1,2} we have developed a method for obtaining first-principles nonlocal atomic pseudopotentials in the density-functional formalism³ by direct inversion of the pseudopotential one-body eigenvalue problem. The method does not involve any empirical data nor does it restrict the pseudopotential to a model analytic form. Applications to excited configurations of atoms and ions as well as to the study of the electronic structure of semiconductors (Si and Ge⁴) and transition metals (Mo,⁵ and⁴ W) has indicated very good agreement with all-electron first-principles calculations. As these pseudopotentials are derived from a variational process that constrains both the energy eigenvalues and the wave functions to reproduce the features of the atomic all-electron one-body equation they are expected to correctly reproduce the band structure and the charge-density related properties of condensed phases.

The classical turning points r_i^0 of the screened core potentials have been shown¹ to constitute a sensitive electronegativity scale reflecting chemical regularities in the Periodic Table. As $(r_i^0)^{-1}$ measures the scattering power of a screened atomic core to valence electrons of angular momentum l , it was possible to construct⁶ "structural indices" for binary AB compounds [i.e.,

$$R_r^{AB} = (r_p^A - r_s^A) + (r_p^B - r_s^B)$$

and

$$R_o^{AB} = (r_p^A + r_s^A) - (r_p^B + r_s^B)]$$

that separate topologically the octet AB structures

(diamond, graphite, zincblende, rocksalt, wurzite, and cesium chloride) as well as the suboctet structures (space groups $L1_0$, $B32$, $B2$, $I64$, and $cp64$). This constitutes the first successful separation of these structures based on a nonempirical approach.

In this paper we apply the first-principle pseudopotentials to the calculation of the total energy and bulk properties of two transition metals, Mo and W. The purpose of this study is to examine the usefulness of these pseudopotentials in revealing not only structural regularities⁶ but also absolute values for structural parameters such as cohesive energy, equilibrium lattice constant, and bulk modulus. In this respect, the choice of the transition metals constitutes a sensitive test because empirical pseudopotentials have been traditionally unsuccessful in describing their electronic properties within a self-consistent approach due to (i) pronounced pseudopotential nonlocality, (ii) the failure of conventional perturbation approaches to treat the localized and strong d potentials, and (iii) the scarcity of empirical data necessary to fit these potentials. On the other hand, an all-electron approach to the cohesive properties of the $4d$ and $5d$ transition elements faces the difficulty associated with the smallness of the cohesive energy relative to the total energy (e.g., 2×10^{-5} in tungsten). A pseudopotential approach, on the other hand, focuses its attention on the "reactive" valence electrons only and hence the cohesive energy constitutes a much larger fraction of the total (valence) energy (e.g., a ratio of 3.6×10^{-2} for tungsten). In the future this might permit extensive structure determinations of complex systems

(transition-metal compounds and surfaces) with reasonable accuracy.

The calculation of the pseudopotential total energy can be greatly facilitated by the use of the momentum-space representation recently developed.⁷ This avoids any muffin-tin approximation to the charge density and replaces the complicated six-dimensional integrals characteristic of first-principles real-space representations⁸⁻¹⁰ by simple and readily convergent reciprocal-space lattice sums. The mixed-basis representation of the crystalline wave functions¹¹⁻¹⁶ similarly permits an accurate description of both the localized and the itinerant features of *d*-band transition metals. The density-functional exchange³ and correlation¹⁷ functionals are used to self-consistently describe the valence screening in the system. As the core pseudopotentials are similarly derived from the density-functional one-body equations,^{1,2} this approach is completely nonempirical and enables a direct assessment of the quality of the presently known local-density exchange and correlation functionals for the description of ground-state properties of transition metals.

II. PSEUDOPOTENTIAL TOTAL ENERGY

The pseudopotential formalism¹⁸ replaces the all-electron (core + valence) eigenvalue problem

$$[-\frac{1}{2}\nabla^2 + V_{\text{tot}}^{c,v}\{\rho(\vec{r})\}] \psi_j(\vec{k}, \vec{r}) = \epsilon_j(\vec{k}) \psi_j(\vec{k}, \vec{r}), \quad (1)$$

where $\psi_j(\vec{k}, \vec{r})$ and $\epsilon_j(\vec{k})$ are the *j*th-band wave function and energy eigenvalue, respectively, and $V_{\text{tot}}^{c,v}\{\rho(\vec{r})\}$ is the total potential (containing electron-nucleus, Coulomb electron-electron, and exchange and correlation terms due to all the electrons), by a simpler equation pertaining to the subspace of the valence electrons only

$$[-\frac{1}{2}\nabla^2 + V^v\{n(\vec{r})\} + V_{\text{ps}}(\vec{r})] \chi_j(\vec{k}, \vec{r}) = \epsilon_j(\vec{k}) \chi_j(\vec{k}, \vec{r}). \quad (2)$$

The all-electron charge density $\rho(\vec{r})$ is given by the core + valence wave functions $\psi_j(\vec{k}, \vec{r})$ as

$$\rho(\vec{r}) = \sum_{j,k} N_j(\vec{k}) |\psi_j^*(\vec{k}, \vec{r}) \psi_j(\vec{k}, \vec{r})|, \quad (3)$$

whereas the pseudo-charge-density $n(\vec{r})$ is similarly constructed from the Fermi-Dirac occupation numbers $N_j(\vec{k})$ and the pseudo-wave-functions $\chi_j(\vec{k}, \vec{r})$ as

$$n(\vec{r}) = \sum_{j,k} N_j(\vec{k}) |\chi_j^*(\vec{k}, \vec{r}) \chi_j(\vec{k}, \vec{r})|. \quad (4)$$

While $\rho(\vec{r})$ contains contributions from $N_c + N_v$ core and valence electrons, $n(\vec{r})$ is normalized to N_v . The valence potential $V^v\{n(\vec{r})\}$ has the same functional form as the total core + valence potential, except that it acts on the valence subspace only.

More specifically, in the density-functional approach,³ it is given as

$$V^v\{n(\vec{r})\} = \sum_{\vec{R}_m} \frac{-Z_v}{|\vec{r} - \vec{R}_m|} + \int \frac{n(\vec{r}')}{|\vec{r} - \vec{r}'|} d\vec{r}' + V_x\{n(\vec{r})\} + V_{\text{corr}}\{n(\vec{r})\}. \quad (5)$$

Here Z_v is the screened nuclear charge of the atom at the lattice point \vec{R}_m and $V_x\{n(\vec{r})\}$, $V_{\text{corr}}\{n(\vec{r})\}$, and $V_{\text{ps}}(\vec{r})$ are, respectively, the local exchange and correlation potentials^{1,17} and the pseudopotential. In general, $V_{\text{ps}}(\vec{r})$ is a nonlocal potential constructed as a lattice sum of the individual single-site pseudopotentials $U_l(\vec{r})$ of angular momentum *l*, as

$$V_{\text{ps}}(\vec{r}, \vec{r}') = \sum_{\vec{R}_m} \sum_{l=0}^{\infty} U_l(\vec{r} - \vec{R}_m, \vec{r}' - \vec{R}_m) \hat{P}_l^{(m)}, \quad (6)$$

where $\hat{P}_l^{(m)}$ is the angular-momentum projection operator with respect to site *m*.

To the extent that the construction of $U_l(\vec{r})$ can be made sufficiently simple, the effective one-body equation (2) is significantly easier to handle than the all-electron equation (1) in that a smaller number of electrons (N_v rather than $N_c + N_v$) has to be treated and the wave functions $\chi_j(\vec{k}, \vec{r})$ can be made spatially smooth (due to the absence of the core orthogonality constraint) and hence are expandable effectively by convenient basis sets. Whereas $U_l(\vec{r})$ has been traditionally treated as an empirically parametrized quantity adjusted to fit either the low-energy interband transitions $\epsilon_j(\vec{k}) - \epsilon_{j'}(\vec{k})$,¹⁹ Fermi surface and resistivity of metals²⁰ or the ionic term values,²¹ we have derived $U_l(\vec{r})$ for all atoms of rows 1-5 in the Periodic Table by a direct inversion of all-electron Eq. (1) in the atomic limit. The construction of the single-site pseudopotentials $U_l(\vec{r})$ from the core characteristics of the free atom, rather than the solid-state core, we are assuming the pseudopotential frozen-core approximation. This implies that the static potential $U_l(\vec{r})$, which replaces exactly the dynamic effects of the core electrons in the *g*th electronic configuration of the atom (i.e., ground state) be used for states other than *g* (e.g., excited states) and for the same core in a polyatomic system. We have previously tested this assumed weak energy dependence of the pseudopotential, studying the electronic structure of atoms,^{1,2} semiconductors,⁴ and transition metals^{4,5} and found that it holds satisfactorily over a considerable energy range. Whereas the empirical fitting of $U_l(\vec{r})$ introduces some form of correlation into the one-body potential and hence obscures the effects of the explicit correlation introduced into the total energy in its density-functional form, the first-principles pseudopotential consistently uses the theoretically transparent correlation func-

tional throughout. This should enable a direct measure to the quality of the presently known many-body correlation functional in predicting ground-state properties of solids. We extend this study presently to the calculation of the total energy and bulk properties of solids.

The total energy associated with the variational equation (2) is given by

$$E_{\text{tot}} = \sum_{j, \vec{k}} N_j(\vec{k}) \epsilon_j(\vec{k}) - \frac{1}{2} \int \int \frac{n(\vec{r})n(\vec{r}')}{|\vec{r} - \vec{r}'|} d\vec{r} d\vec{r}' - \int n(\vec{r}) [V_x(\vec{r}) + V_{\text{corr}}(\vec{r})] d\vec{r} + E_{xc}\{n(\vec{r})\} + \sum_{m \neq n} \frac{Z_v^2}{|\vec{R}_m - \vec{R}_n|} \quad (7)$$

and does not depend explicitly on the pseudopotential. Expressing the total exchange and correlation energy $E_{xc}\{n(\vec{r})\}$ by its approximate density-functional form³

$$E_{xc}\{n(\vec{r})\} \cong \int n(\vec{r}) \epsilon_{xc}\{n(\vec{r})\} d\vec{r}, \quad (8)$$

where $\epsilon_{xc}\{n(\vec{r})\} = \epsilon_x\{n(\vec{r})\} + \epsilon_c\{n(\vec{r})\}$ is the exchange and correlation energy per particle, which is related to the corresponding one-body potentials by

$$V_x\{n(\vec{r})\} = \frac{4}{3} \epsilon_x\{n(\vec{r})\}, \quad (9)$$

$$V_{\text{corr}}\{n(\vec{r})\} = \epsilon_c\{n(\vec{r})\} + n(\vec{r}) \frac{d\epsilon_c\{n(\vec{r})\}}{dn(\vec{r})}$$

one obtains the expression for E_{tot} expressed by direct-space quantities as

$$E_{\text{tot}} = \sum_{j, \vec{k}} N_j(\vec{k}) \epsilon_j(\vec{k}) - \frac{1}{2} \int \int \frac{n(\vec{r})n(\vec{r}')}{|\vec{r} - \vec{r}'|} d\vec{r} d\vec{r}' - \frac{1}{4} \int n(\vec{r}) V_x(\vec{r}) d\vec{r} + \int n(\vec{r}) [\epsilon_c\{n(\vec{r})\}] - V_{\text{corr}}\{n(\vec{r})\} d\vec{r} + \sum_{m \neq n} \frac{Z_v^2}{|\vec{R}_m - \vec{R}_n|}. \quad (10)$$

The first term is the sum of the one-body eigenvalues over the occupied portion of the Brillouin zone (BZ), while the second term is the correction due to the overcounting of the interelectronic Coul-

omb repulsion. The third and fourth terms are corrections to the exchange and correlation energies, respectively, while the last term is the core-core nuclear repulsion term. The corresponding equation pertaining to all the all-electron case [Eq. (1)] is formally identical with Eq. (10) when the pseudo charge density $n(\vec{r})$ is replaced by the all-electron density $\rho(\vec{r})$ and the valence charge Z_v is replaced by the atomic number Z .

In practice it appears to be difficult to obtain E_{tot} for a solid directly from Eq. (10) for the general case where $n(\vec{r})$ [or $\rho(\vec{r})$] is unrestricted to simple model forms (viz. the muffin-tin approximation), both due to the occurrence of the six-dimensional integral in the second term in Eq. (10) and due to the divergent nature of the second and last term in Eq. (10). It has been demonstrated in the past²²⁻²⁵ that when $n(\vec{r})$ [or $\rho(\vec{r})$] is approximated by a radially one-dimensional quantity (e.g., muffin-tin or cellular density), one can reduce all the spatial integrals in Eq. (10) into simple one-dimensional integrals and combine the individually divergent terms to yield a converged expression. Whereas the former approximation seems to apply reasonably well to closely packed structure, there is increasing evidence²⁶⁻²⁸ that similar approximations for "open" molecular and solid-state systems involve very large errors both in the single-particle energies in Eqs. (1) and (2) and in the total energy in Eq. (10). Direct non-muffin-tin evaluations of Eq. (10) for open-structure solids has been nevertheless achieved both in the restricted Hartree-Fock method^{8, 9, 29} and in the density-functional approach^{10, 30, 31} yielding very good agreement with the observed bulk properties. The pseudopotential approach offers an alternative scheme, within the frozen-core approximation, which simplifies the calculation enormously without sacrificing the variational form of $n(\vec{r})$. This is based on a momentum-space representation of Eq. (10) which becomes readily convergent due to the spatial smoothness of $\chi_j(\vec{k}, \vec{r})$ [as opposed to the nodal character of $\psi_j(\vec{k}, \vec{r})$], replaces all integrals by single sums and eliminates all the individual divergencies in E_{tot} . This formalism, previously developed by Ihm, Zunger, and Cohen⁷ yields a simple expression for the total energy per cell, as

$$E_{\text{tot}} = \sum_{j, \vec{k}} N_j(\vec{k}) \epsilon_j(\vec{k}) - \sum_{\vec{G}}^{G(1)} n(\vec{G}) [V_{\text{Coul}}(\vec{G}) + V_x(\vec{G}) + V_{\text{corr}}(\vec{G})] + \frac{1}{2} \sum_{\vec{G}}^{G(1)} n(\vec{G}) V_{\text{Coul}}(\vec{G}) + \frac{3}{4} \sum_{\vec{G}}^{G(1)} n(\vec{G}) V_x(\vec{G}) + \sum_{\vec{G}}^{G(1)} n(\vec{G}) \epsilon_c(\vec{G}) + \sum_{\beta} \alpha^{(\beta)} Z_v^{(\beta)} + E_{\text{Ewald}} = \sum_{j, \vec{k}} N_j(\vec{k}) \epsilon_j(\vec{k}) - \frac{1}{2} \sum_{\vec{G} \neq 0}^{G(1)} V_{\text{Coul}}(\vec{G}) n(\vec{G}) - \frac{1}{4} \sum_{\vec{G} \neq 0}^{G(1)} V_x(\vec{G}) n(\vec{G}) + \sum_{\vec{G} \neq 0}^{G(1)} [\epsilon_c(\vec{G}) - V_{\text{corr}}(\vec{G})] n(\vec{G}) + \sum_{\beta} \alpha^{(\beta)} Z_v^{(\beta)} + E_{\text{Ewald}}. \quad (11)$$

Here V_{Coul} denotes the electron-electron repulsion term [second term in Eq. (5)], $\alpha^{(6)}Z_v^{(6)}$ is the $\vec{G}=0$ component of the repulsive local pseudopotential of atom β , and E_{Ewald} is the Ewald core-core energy.³² The primed sums indicate omission of the $\vec{G}=0$ term from $V_{\text{Coul}}(\vec{G})$ and $G_{\text{max}}^{(1)}$ denote the summation limit. The local pseudopotential is defined by arbitrarily partitioning $V_{\text{ps}}(\vec{r})$ into a term acting equally on all the angular-momentum components of the wave function [$V_L(\vec{r})$] and a term which acts differently on each component [$V_{\text{NL}}(\vec{r})$]. Using the completeness of P_l one obtains

$$\begin{aligned} V_{\text{ps}}(r) &= V_L(\vec{r}) + V_{\text{NL}}(\vec{r}) \\ &= \sum_{\vec{R}_m, \tau_\beta} U_L(\vec{r} - \vec{R}_m - \tau_\beta) \\ &\quad + \sum_{\vec{R}_m, \tau_\beta} \sum_l [U_l(\vec{r} - \vec{R}_m - \tau_\beta) - U_L(\vec{r} - \vec{R}_m - \tau_\beta)] \\ &\quad \times P_l^{(m, \beta)}. \end{aligned} \quad (12)$$

This partitioning turns out to be of practical importance in solving the eigenvalue problem Eq. (2) without sacrificing the generality of the method. In terms of $U_L(\vec{r})$ and the cell volume Ω , the $\vec{G}=0$ first-order component is given simply as

$$\alpha^{(6)}Z_v^{(6)} = \frac{Z_v^{(6)}}{\Omega} \int U_L^{(6)}(\vec{r}) d\vec{r}. \quad (13)$$

The total energy in its momentum-space representation is exceedingly simple to evaluate as long as the convergence of the relevant reciprocal-space single sums is fast. It constitutes an improvement over the perturbational approaches,³³⁻³⁵ which assume the smallness of the low-momentum-potential Fourier components and simple forms for the dielectric screening. The major advantage of the momentum-space representation for E_{tot} over the real-space representation lies in the absence of complicated multidimensional and multi-center integrals in the former. We discuss in Sec. III the convergence properties of both the eigenvalue problem (2) and the total energy expression (11).

III. CONVERGENCE PROPERTIES

A. One-body equation

As the accuracy of the total energy will be largely determined by the corresponding accuracy of the charge density $n(\vec{r})$ and the eigenvalue spectra $\epsilon_j(\vec{k})$ obtained from the one-body equations (2) and (4), we first discuss the convergence properties of the latter.

In order to be able to treat systems that might

contain localized states as well as extended states (e.g., transition metals) without having to artificially smooth the pseudopotential, the crystal wave function $\chi_j(\vec{k}, \vec{r})$ is expanded in a mixed representation of plane waves and localized linear-combination-of-atomic-orbitals (LCAO) Bloch functions¹¹

$$\begin{aligned} \chi_j(\vec{k}, \vec{r}) &= \sum_{\vec{G}}^{G_{\text{max}}^{(2)}} C_{\vec{k}+\vec{G}}^{(j)} e^{i(\vec{k}+\vec{G})\cdot\vec{r}} \\ &\quad + \sum_{\mu} \sum_{\alpha} D_{\mu\alpha}^j(\vec{k}) \Phi_{\mu\alpha}(\vec{k}, \vec{r}). \end{aligned} \quad (14)$$

Here $C_{\vec{k}+\vec{G}}^{(j)}$ and $D_{\mu\alpha}^j(\vec{k})$ denote the expansion coefficients to be determined variationally and $\Phi_{\mu\alpha}(\vec{k}, \vec{r})$ denotes a Bloch function constructed from the real-space basis orbitals $d_{\mu\alpha}(r)$ of type μ on sublattice α (located at $\vec{\tau}_\alpha$), as

$$\Phi_{\mu\alpha}(\vec{k}, \vec{r}) = \sum_{\vec{R}_m} e^{i\vec{k}\cdot\vec{R}_m} d_{\mu\alpha}(\vec{r} - \vec{R}_m - \vec{\tau}_\alpha). \quad (15a)$$

The basis orbitals $d_{\mu\alpha}(r)$ are chosen here as a linear combination of Gaussians

$$d_{\mu\alpha}(r) = N_{lm} r^l K_{lm}(\theta, \rho) \sum_t a_{lm\alpha}^{(t)} e^{-r_t r^2}, \quad (15b)$$

where N_{lm} is a normalization, $K_{lm}(\theta, \rho)$ are the Kubic harmonics of angles θ , and ρ and μ denotes l and m , collectively. As the matrix representation of $\Phi_{\mu\alpha}(\vec{r})$ is obtained in momentum space, it is possible to use Slater-basis functions as well as Gaussians (due to the analyticity of their Fourier representations) without additional complexity. The coefficients $a_{lm\alpha}^{(t)}$ are determined from the outset such that $d_{\mu\alpha}(r)$ have desired properties (e.g., fit the atomic pseudo wave functions at small distances from the origin).

In order to apply the powerful momentum-space techniques to the evaluation of the matrix representation of the Hamiltonian, the localized Bloch functions are expressed themselves in plane waves

$$\Phi_{\mu\alpha}(\vec{k}, \vec{r}) = M^{-1/2} \sum_{\vec{G}}^{G_{\text{max}}^{(3)}} e^{i(\vec{k}+\vec{G})\cdot\vec{r}} d_{\mu\alpha}(\vec{k}+\vec{G}) T_\alpha(\vec{G}), \quad (16)$$

where $M^{-1/2}$ is a normalization constant, $d_{\mu\alpha}(\vec{k}+\vec{G})$ is the Fourier transform of the basis orbital $d_{\mu\alpha}(r)$ [Eq. (15)], and $T_\alpha(\vec{G})$ is the structure factor

$$T_\alpha(\vec{G}) = \sum_p e^{-\vec{G}\cdot\vec{\tau}_{\alpha,p}} \quad (17)$$

obtained by summing all phase factors related to the p atoms of type α . The crystalline wave functions are then given in a Fourier representation as

$$\chi_j(\vec{k}, \vec{r}) = \sum_{\vec{G}} C_{\vec{k}+\vec{G}}^{(j)} e^{i(\vec{k}+\vec{G})\cdot\vec{r}} + \sum_{\vec{G}'} \left(\sum_{\mu, \alpha} D_{\mu\alpha}^{(j)}(\vec{k}) d_{\mu\alpha}(\vec{k}+\vec{G}') T_{\alpha}(\vec{G}') \right) \times e^{i(\vec{k}+\vec{G}')\cdot\vec{r}}. \quad (18)$$

Within the form (18), it is very simple to evaluate the matrix elements of the Hamiltonian components simply as lattice sums. Some examples are given in Appendix A. These involve simple summations in momentum space and require the knowledge of the Fourier components of the local potential $V_L(\vec{G})$ as well as the spherical Bessel matrix elements of the nonlocal potential $V_{NL}(\vec{G}, \vec{G}')$. These are easily evaluated as one-dimensional numerical radial integrals. The upper limits $G_{\max}^{(2)}$ and $G_{\max}^{(3)}$ denote the momentum of the highest Fourier component of the plane wave and LCAO Bloch function, respectively. As, however, the size of the secular equation to be solved is determined by $G_{\max}^{(2)}$ and the number h of LCAO Bloch function, one can increase $G_{\max}^{(3)}$ in Eqs. (16) and (18) without increasing the matrix size.

The secular equation is solved on a grid of \vec{k}_p points in the Brillouin zone. The resulting wave functions $\chi_j(\vec{k}_p, \vec{r}_i)$ are constructed from Eq. (18) on a grid \vec{r}_i in real space (using fast-Fourier transform³⁶) and used in a symmetrized form to evaluate the charge density in Eq. (4),

$$n(\vec{r}_i) = \sum_j \sum_{\vec{k}_p}^{N_k} W_j(\vec{k}_p) |\chi_j^*(\vec{k}_p, \vec{r}_i) \chi_j(\vec{k}_p, \vec{r}_i)|. \quad (19)$$

Here $W_j(\vec{k}_p)$ denotes band and wave-vector dependent weights. Whereas in insulators and semiconductors it is possible to use the "special \vec{k} points"³⁷ (which are band independent), for metals one has to incorporate explicitly the variations in the weights of various bands at a given point \vec{k}_p due to its position relative to the Fermi surface.⁴ This is done by the tetrahedron scheme³⁸ in which we divide the BZ into tetrahedra, evaluating the band structure for all corner points and using these to calculate the density of states and Fermi energy. The weights $W_j(\vec{k}_p)$ are then determined from the fraction of each tetrahedron which lies under the Fermi energy, for each band. At each self-consistency iteration step the Fermi energy, density of states and weights $W_j(\vec{k}_p)$ are recalculated.

Using the density $n(\vec{r}_i)$ we evaluate the exchange and correlation potentials $V_x\{n(\vec{r}_i)\}$ and $V_{\text{corr}}\{n(\vec{r}_i)\}$ on the same grid. These are then fast-Fourier transformed³⁶ into their momentum representation

$$V_x(\vec{r}_i) = \sum_{\vec{G}}^{G_{\max}^{(4)}} e^{i\vec{G}\cdot\vec{r}_i} V_x(\vec{G}), \quad (20)$$

$$V_{\text{corr}}(\vec{r}_i) = \sum_{\vec{G}}^{G_{\max}^{(4)}} e^{i\vec{G}\cdot\vec{r}_i} V_{\text{corr}}(\vec{G}),$$

as well as

$$n(\vec{r}_i) = \sum_{\vec{G}}^{G_{\max}^{(4)}} e^{i\vec{G}\cdot\vec{r}_i} n(\vec{G}). \quad (21)$$

The momentum components of the electrostatic potential are then given by

$$V_{\text{Coul}}(\vec{G}) = 4\pi m(\vec{G})/\vec{G}^2. \quad (22)$$

The divergent $\vec{G}=0$ component of $V_{\text{Coul}}(\vec{G})$ is set arbitrarily to zero. This is compensated for in the total energy expression through the term αZ_p .⁷ This updated crystal screening potential, {which is identical to the valence field V^v [Eq. (5)], omitting the nuclear attraction}

$$V_{\text{scr}}(\vec{G}) = V_{\text{Coul}}(\vec{G}) + V_x(\vec{G}) + V_{\text{corr}}(\vec{G}), \quad (23)$$

together with the known Fourier components of the local $[V_L(\vec{G})]$ and nonlocal $[V_{NL}(\vec{G}, \vec{G}')]$ pseudopotential (where the nuclear attraction term is absorbed into V_L) are used to determine the band structure repeatedly, until the agreement in these components in successive iterations is better than a prescribed tolerance of 10^{-5} Ry.

The convergence problems that govern the accuracy of the self-consistent band structure are the (i) number of plane waves (with cutoff $G_{\max}^{(2)}$) used to expand the crystal wave functions, the number h of LCAO Bloch functions, and number of plane waves (with cutoff $G_{\max}^{(3)}$) used to expand each such Bloch function [Eq. (18)]. (ii) number N_k of \vec{k}_p points used to sample the BZ for computing the charge density [Eq. (19)], (iii) number of components used to expand the potential and charge density [Eqs. (10) and (21)], and (iv) tolerance criteria for achieving self-consistency.

The size of the basis set (1) depends on the degree to which the LCAO basis functions are optimized. A judicious choice of the Gaussian exponents γ_i and contraction coefficients $a_{l m \alpha}^{(i)}$ [Eq. (15)] would lead to a smaller $G_{\max}^{(2)}$ as more of the high momentum components of the crystalline wave functions are described by the localized orbitals. Whereas very large exponents (i.e., tightly bound Gaussians) would require a high cutoff $G_{\max}^{(3)}$ for their Fourier representation [Eq. (16)], unduly small exponents (i.e., diffused Gaussians) might lead to approximate linear dependence between the LCAO Bloch functions and the long wavelength plane waves. In the present study of Mo and W we use a single Gaussian for the localized Bloch function

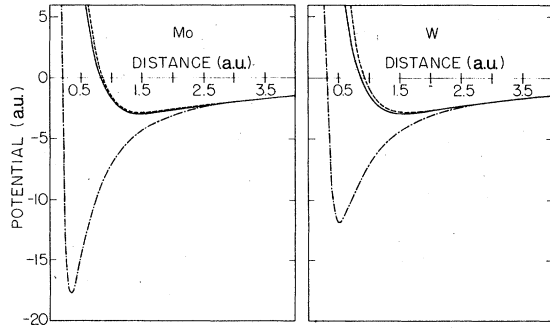


FIG. 1. First-principles nonlocal core pseudopotentials $U_1(r) - Z_v/r$ for molybdenum and tungsten. Solid line: $l=0$; dashed line: $l=1$; dashed-dotted line: $l=2$.

[i.e., $i=1$, $l=2$, and $-2 \leq m < 2$ in Eq. (15b)] and choose the exponent γ_i such that the basis function $d_{i\alpha}(\vec{r})$ match the initial rise of the exact numerical $4d$ or $5d$ atomic *pseudoorbitals*. We then use $G_{\max}^{(2)}$ in Eq. (18) as a convergence parameter, increasing it until all energy eigenvalues containing d character stabilize to within 0.01 eV. It turns out that approximate linear dependence (monitored by the smallness of the eigenvalues of the overlap matrix³⁹) does not occur within this choice, up to very high values for $G_{\max}^{(2)}$. For this choice, $\gamma_{\text{Mo}} = 1.9$ a.u.⁻² and $\gamma_{\text{W}} = 1.4$ a.u.⁻², an accuracy of 0.01 eV or better in the energy eigenvalues requires $|G_{\max}^{(2)}|^2 = 15$ Ry (or about 110–140 plane waves) and $|G_{\max}^{(3)}|^2 = 55$ Ry (or 730 plane waves). For comparison, a calculation using a pure plane-waves basis [i.e., $a_{i\alpha}^{(4)} \equiv 0$ in Eq. (15b)] a comparable accuracy requires 430 plane waves in the basis. These high cutoff values are required both due to the relatively localized nature of the d potential $U_2(\vec{r})$ (Fig. 1) and the needed high precision in $\epsilon_j(\vec{k})$ for a total energy calculation. An accuracy of 0.1 eV, in the energy eigenvalues more akin to regular band-structure calculations, can be achieved with $|G_{\max}^{(2)}|^2 = 11$ Ry (about 70 plane waves).

The grid of N_k points in the BZ used to sample the wave functions $\chi_j(\vec{k}, \vec{r})$ [Eq. (19)] poses a difficult convergence problem: Whereas in the cubic

semiconducting systems such as Si and Ge the orbital character of the wave functions $\chi_j(\vec{k}, \vec{r})$ changes smoothly across the Brillouin zone,⁴ the hybridization in the cubic transition metals has a much stronger dispersion,^{4,5} requiring a larger number of \vec{k}_p points for adequate sampling. We find that the eight special \vec{k}_p points³⁷ are insufficient for obtaining the relevant accuracy in $\sum_{j,k} N_j(\vec{k}) \epsilon_j(\vec{k})$ and $n(\vec{r}_i)$. Comparing the eigenvalue sum and the charge density obtained with 14 and 20 \vec{k}_p points, we find maximal differences of only 0.03 eV and 0.2%, respectively.

Table I demonstrates the convergence rate of the components of the screening field $V_{\text{Coul}}(\vec{r}_i)$, $V_x(\vec{r}_i)$, and $V_{\text{corr}}(\vec{r}_i)$ in tungsten, as a function of the number of plane wave [with cut-off $G_{\max}^{(4)}$ in Eqs. (20) and (21)] included in the sum. For comparison, similar results are shown for the local pseudopotential $V_L(\vec{r}_i)$. As these materials are characterized by very large low-momentum-density component (e.g., $n([111]) = 0.67 e/\text{cell}$ in W) with a very large number of equally small high momentum components the convergence rate is relatively slow. Figure 2 shows the variation in the screening field components along the [111], [110], and [100] directions in tungsten as well as that of the local pseudopotential (with inclusion of the Z_v/r term in it). It is obvious that the correlation potential is almost constant over large portions of the unit cell space and hence has a rapid convergence in momentum space (Table I), whereas the steep nature of the core potential close to its classical turning points results in a much slower convergence rate. The Coulomb screening shows appreciable spatial variations in the solid and about 1200 waves are required to converge it in momentum space. About 1500 waves are similarly required to converge the charge density.

Whereas an accurate determination of the total crystal energy is found to require highly converged pseudopotentials and screening fields, we find that no such high cutoff values are required to determine the relative values of the band structure

TABLE I. Convergence of the Coulomb, exchange, correlation, and local pseudopotential at the body-centered atomic site ($\vec{r} = \vec{\tau}$) of tungsten, as a function of the number of plane waves. Results are given in Ry.

No. of waves	$\sum_{\vec{G} \neq 0} V_{\text{Coul}}(\vec{G}) e^{i\vec{G} \cdot \vec{\tau}}$	$\sum_{\vec{G}} V_x(\vec{G}) e^{i\vec{G} \cdot \vec{\tau}}$	$\sum_{\vec{G}} \epsilon_c(\vec{G}) e^{i\vec{G} \cdot \vec{\tau}}$	$\sum_{\vec{G} \neq 0} V_L(\vec{G}) e^{i\vec{G} \cdot \vec{\tau}}$
250	0.8918	-0.3389	-0.0865	42.3440
500	0.8677	-0.1427	-0.0644	51.8192
750	0.8751	-0.1593	-0.0652	56.0236
1000	0.8785	-0.1438	-0.05963	58.3250
1250	0.8829	-0.1112	-0.04891	60.6941
1500	0.8825	-0.1104	-0.04808	60.6958

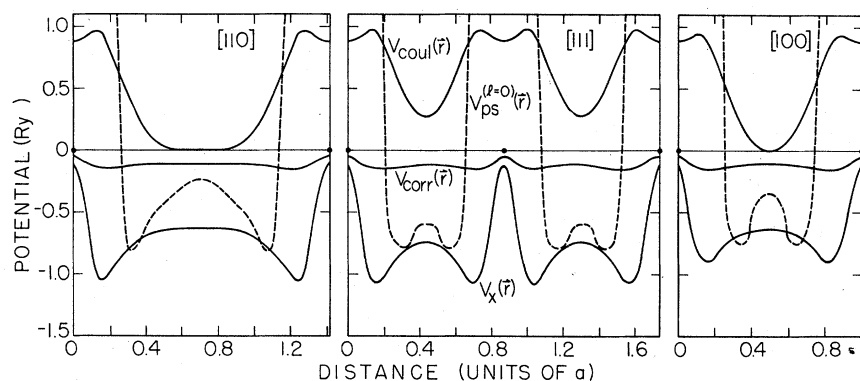


FIG. 2. Spatial variation of the self-consistent screening potential (Coulomb, V_{Coul} ; exchange, V_x ; and correlation, V_{corr}) and the local core pseudopotential $V_{\text{ps}}^{(l=0)}$ for bcc tungsten. Full circles indicate atomic positions. The zero is chosen as the Fermi energy.

$\epsilon_j(\vec{k})$. A calculation involving only 750 plane waves for the potential expansion produced a band structure $\epsilon_j(\vec{k}) - \epsilon_{\Gamma_1}$ (where Γ_1 is the bottom of the valence band) that deviated by less than 0.1 eV from that obtained with converged potentials. At the same time, a sizeable (1.5 eV) rigid shift occurs for the center of gravity of the bands $N^{-1} \sum_{j,k} \epsilon_j(\vec{k})$. While such a nearly dispersionless shift is usually unimportant for the purpose of calculating one-electron properties such as the Fermi surface and interband spectra, it is not compensated for by the $\vec{G}=0$ components of the core and Coulomb potentials and hence directly affects the total energy of the system. Hence, while the band structure is determined primarily by scattering events that exchange momentum of the order of $\approx 2\vec{k}_F$ (where \vec{k}_F is the Fermi momentum), the total energy is determined also by the $\vec{G}=0$ component [viz., αZ_v in Eqs. (11) and (13)] as well as by high momentum scattering events in which the electrons sample the repulsive portions of the potential near its classical turning points (Fig. 2).

The last convergence problem associated with the one-body equation pertains to the self-consistency iterative procedure. The first iteration in solving Eq. (2) is usually carried out by replacing the screening field in Eq. (23) by the corresponding quantities calculated from the free-atom pseudowave functions, in a chosen electronic configuration. As observed earlier in non-self-consistent augmented-plane-wave (APW⁴⁰) and cellular⁴¹ studies on transition metals, the choice of the electronic configuration (e.g., $\text{Mo}4d^{5-9}5s^{1+Q}$ and $\text{W}5d^{5-9}6s^{1+Q}$, where $0 \leq Q \leq 1$) determines rather sensitively many of the important features of the band structure, including the s - d and p - d separations, etc. In the present fully self-consistent study, this choice is immaterial. We find that if one starts from a superposition of ground-state atoms (i.e., $Q=0$), the self-consistency considerably modifies the relative positions of the bands, and in particular (i) the s - d gap Γ_1 - H_{12} is reduced

by about 0.3 eV, (ii) the p - d splitting at N_1 - N_1 , is reduced by about 0.5 eV, (iii) the $d_{x^2-y^2}$ - $d_{x^2-y^2}$ gap at P_4 - H_{12} is reduced by 0.8 eV, and (iv) the bonding-antibonding gap (Γ_{12} with the upper Γ_{25} state) is increased by about 3 eV. Corrections (i) and (iii) improve the agreement with the Fermi surface data⁴ whereas correction (ii) improves the agreement with the photoemission results⁴ and correction (iii) acts to further polarize the charge density in the directions of the bonds (i.e., the four charge-density maxima at $\frac{1}{5}a$ from the origin in Fig. 3 are substantially enhanced) thereby stabilizing the crystal electrostatically. Although similar effects can be simulated in a non-self-consistent study by empirically adjusting the potential,^{43,44} such procedures seem intractable when applied to the total energy.

The requirement of establishing a self-consistent solution to the one-particle equation is even more stringent in the context of a total energy calculation: expressions (10) and (11) for the total energy make use of the fact that the screening

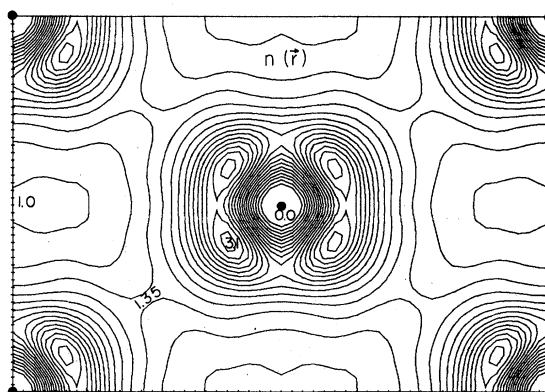


FIG. 3. Self-consistent valence pseudocharge density of tungsten in the [110] plane. Full circles indicate the atomic positions. The charge values are given in $e/a.u.^3$, normalized to unity.

field $V_{\text{Coul}} + V_x + V_{\text{corr}}$ in these equations [derived from the variational charge density through Eqs. (20) and (22)] is in fact identical to that used in the one-body Eq. (2). If the potential V_p used in Eq. (2) ($V_p = V_{\text{Coul}}^{\text{old}} + V_x^{\text{old}}$) is different from that derived from the variational density ($V_{\text{Coul}}^{\text{new}} + V_x^{\text{new}}$), the second and third terms in (11) read

$$E_{\text{Coul}} + E_x = \sum_{\vec{G} \neq 0} n(\vec{G}) \left[\frac{1}{2} V_{\text{Coul}}^{\text{new}}(\vec{G}) - V_{\text{Coul}}^{\text{old}}(\vec{G}) \right] + \sum_{\vec{G}} n(\vec{G}) \left[\frac{3}{4} V_x^{\text{new}}(\vec{G}) - V_x^{\text{old}}(\vec{G}) \right]. \quad (24)$$

Hence, non-self-consistent total energy calculations using forms such as Eq. (11)⁴² should be treated with great caution.

We find that six to eight (damped) iterations are required to achieve a stability of 10^{-5} Ry or better in the components of the screening potential in Eq. (23). Whereas the energy eigenvalues are already stabilized to within 0.03 eV at a self-consistency tolerance of 10^{-3} Ry, the high momentum components which determine the spatial anisotropy of the screening potential and the total energy stabilize only after a few more iterations.

The only quantities involved in the solution of the one-body equations which require integrations are the Fourier transforms $d_{\mu\alpha}(\vec{G})$ of the Gaussian basis functions [Eq. (16)], the local potential $V_L(\vec{G})$, and the spherical Bessel matrix elements $U_l(\vec{G}, \vec{G}')$

(Appendix A). The first quantity is evaluated analytically whereas $V_L(\vec{G})$ and $U_l(\vec{G}, \vec{G}')$ require one-dimensional numerical radial integration. These can be performed with great accuracy using Gauss quadrature schemes.

We conclude that the convergence tolerances for the energy eigenvalues and charge density, required for adequate total energy calculations are almost an order of magnitude smaller than these pertinent to "standard" band-structure calculations. This accuracy in the solution of the one-body problem can be conveniently achieved within the mixed basis representation even for transition metals.

B. Total-energy equation

The calculation of the total energy in its momentum-space representation [Eq. (11)] involves the stabilization of the coulomb, exchange, and correlation energies as a function of the kinetic energy cutoff $|G_{\text{max}}^{(l)}|$. Table II demonstrates the convergence properties of these energies. We show for comparison also the convergence of the local core potential energy. This quantity does not appear in the total energy but forms a part of the kinetic as well as the potential energy.

We find that about 1300 waves are necessary to stabilize all three components of the screening field to within 10^{-5} Ry whereas 200 more waves are necessary to reach a similar convergence in the core pseudopotential energy.

TABLE II. Convergence of the electrostatic, exchange, correlation, and core energies for tungsten (in Ry) as a function of the number of Fourier components [or kinetic energy cut-off $|G_{\text{max}}^{(l)}|$ in Eq. (11)] used. Values pertain to the calculated equilibrium lattice parameter.

No. of waves	Kinetic energy $ G_{\text{max}}^{(l)} ^2$	$\sum_{\vec{G} \neq 0} n(\vec{G}) V_{\text{elect}}(\vec{G})$	$\sum_{\vec{G}} n(\vec{G}) V_x(\vec{G})$	$\sum_{\vec{G}} n(\vec{G}) \epsilon_c(\vec{G})$	$\sum_{\vec{G} \neq 0} n(\vec{G}) V_{\text{ps}}^{(l=0)}(\vec{G})$
1	0.0000	0.0000	-4.4465	-0.6248	0.0000
13	2.2142	0.6099	-4.6537	-0.6352	3.6479
19	4.4285	0.6100	-4.6544	-0.6352	3.5894
43	6.6427	0.6110	-4.6566	-0.6354	3.3167
55	8.8569	0.6129	-4.6598	-0.6356	3.0742
79	11.0712	0.6286	-4.6852	-0.6369	2.1658
87	13.2855	0.6289	-4.6858	-0.6369	2.1051
135	15.4997	0.6330	-4.6953	-0.6375	1.5811
141	17.7139	0.6352	-4.7003	-0.6377	1.4609
177	19.9782	0.6389	-4.7104	-0.6383	1.1337
201	22.1425	0.6402	-4.7145	-0.6385	0.9885
225	24.3567	0.6402	-4.7148	-0.6385	0.9678
249	26.5709	0.6403	-4.7152	-0.6386	0.9381
	
1289	79.7129	0.64142	-4.71934	-0.63875	0.85729
1409	81.9272	0.64141	-4.71931	-0.63875	0.85782
1433	84.1415	0.64141	-4.71931	-0.63875	0.85804
1481	86.3557	0.64141	-4.71931	-0.63875	0.85833
1505	88.5699	0.64141	-4.71931	-0.63875	0.85833

The repulsive local potential energy αZ_v [Eq. (13)] is computed numerically as a one-dimensional integral, with almost arbitrary accuracy. The Ewald energy E_{Ewald} is obtained as a simple function of the valence charge and unit-cell volume³² and is readily available to six significant figures. We conclude that the calculation of the total energy [Eq. (11)] poses no practical difficulty if a suitably converged band structure is given.

IV. RESULTS

A. Screening field and charge density

The self-consistent valence pseudo-charge-density of W is shown in the [110] plane in Fig. 3. The charge is seen to be strongly unisotropic with four equivalent maxima around each atom (at a distance of $\frac{1}{5}a$) and a more uniform metalliclike density at the cell boundaries. The results for molybdenum are qualitatively similar⁵ except that the relative heights of the charge maxima are increased to $4.3 e/\text{a.u.}^3$ due to the stronger d potential (Fig. 1). The four maxima shown reflect predominantly the $d_{xy, yz, zx}$ character of the occupied bands, whereas the polarization of the charge density inwards to these lobes reflects the admixture of d_{z^2} character. The nearly constant density at the cell boundaries is due to the s - p components of the charge density. We find very advanced s - d as well as p - d hybridization in the system, as reflected by the charge densities of individual band as well as by the small s - d and p - d energy separations.

The spatial variations in the self-consistent screening fields along the [111], [110], and [100] directions is shown in Fig. 2. It is interesting to note that while both the exchange and the correlation screening potentials have an absolute minimum at a distance of $\frac{1}{5}a$ from the atomic sites, the Coulomb screening has an absolute maximum at these points whereas the core potential has its minimum at about $\frac{1}{3}a$. The extrema of the Coulomb, exchange and correlation potentials are closely related to the occurrence of a high density of d electrons at a distance of $\frac{1}{5}a$ from the atomic sites (c.f. Fig. 3) whereas the minimum of the core pseudopotential at $\frac{1}{3}a$ is determined solely by the core properties [through the variational calculation¹ of $U_i(r)$] and the crystal packing [through the lattice summation in Eq. (6)]. This results in an effective screening of the interelectronic Coulomb interactions by the exchange and correlation fields over large portions of the unit cell, whereas the electron-core interactions are screened effectively only within the core radius ($\bar{r} < \frac{1}{3}a$) where the tightly bound and directional d -electrons charge density is dominant. Note that the repulsive nature of the local ($l=0$) pseudopotential (Fig. 2)

leads to only very small amplitudes of the valence s -type pseudo-wave-functions at the core region, while $l \neq 0$ character can effectively penetrate this region because of the weaker nonlocal pseudopotentials. As the double-well structure of the electron-core potential occurs away from the extrema of the screening potentials, it gives rise to unconnected "islands" in the bond charge (cf. Fig. 3). This is in contrast with the situation encountered in covalently bonded materials⁴ where the less localized core potential is effectively screened in the bond center leading to the formation of a single (distorted) charge-density ellipsoid along the interatomic axis, constituting the covalent bond.

In a previous study^{6a} we have demonstrated that the classical turning points r_l of the *atomically* screened first-principles pseudopotentials constitute accurate structural indices, capable of providing with an essentially exact separation of the various stable phases of *solids* in both octet and suboctet structures. These turning points (cf. Fig. 1) are strongly l dependent but spatially isotropic and vary in a systematic way across the Periodic Table.^{4,6} It has been unclear, however, if these radii remain as good "quantum indices" when the self-consistent screening in the *solid*, as well as the directional anisotropy of the core potential in the condensed phase, are taken into account. The calculation of the classical turning points of the screened potential in the solid is, however, complicated by the fact that both $V_{ps}^{(l)}(\bar{r})$ and $V_{\text{Coul}}(\bar{r})$ cannot be easily referred to a common vacuum level due to the omission of their divergent $\vec{G}=0$ component. Although these components are individually divergent, their sum is a constant which constitutes the correction to the work function calculated from Eq. (2). This correction is of the order of ~ 5 eV in Mo.⁴⁵ Figure 2 shows, however, that the classical turning points are largely insensitive to such small variations in the zero of the potential. Using the difference between the observed work function and our calculated Fermi energy as a rough measure to this zero energy shift we find that the $l=0$ turning points for tungsten are 1.279 ± 0.002 a.u. along the [111] direction, 1.214 ± 0.002 a.u. along the [001] direction, and 1.256 ± 0.002 a.u. along the [110] direction, where the error bars refer to charges of the zero of $V_{ps}^{(l)}(\bar{r}) + V_{\text{Coul}}(\bar{r})$ by ± 5 eV. The values obtained for bulk Mo are, respectively, 1.229 ± 0.001 , 1.217 ± 0.002 , and 1.221 ± 0.002 a.u. We see that the maximum spatial anisotropy of the turning point as a fraction of the average values is 2.9% for W and 0.7% in Mo. The average values of 1.25 a.u. in W and 1.22 a.u. in Mo are indeed close to the values obtained from the *atomically* screened potentials¹ (1.225 and 1.215 a.u. in W and Mo, respec-

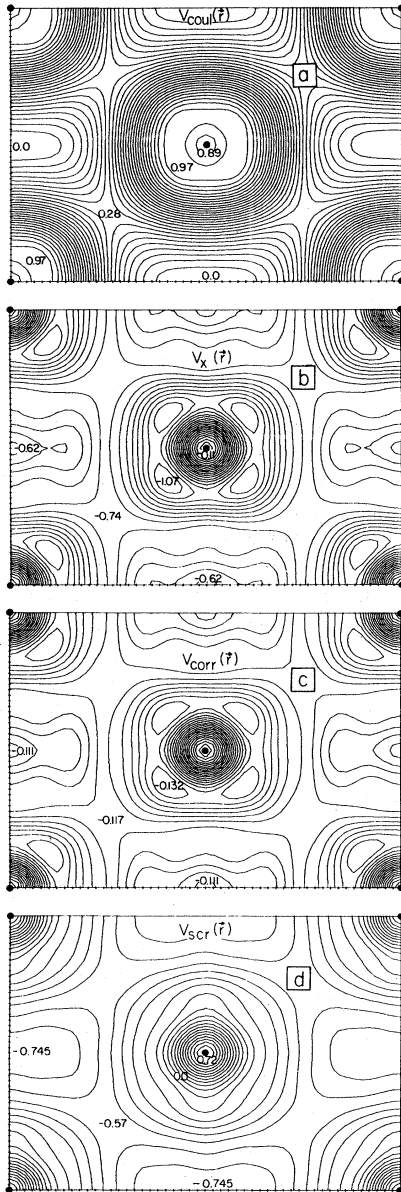


FIG. 4. Contour plot of the (a) Coulomb, (b) exchange; (c) correlation, and (d) total screening of tungsten in the [110] plane. Full circles denote atomic positions. Energy values are given in Ry.

tively), confirming thereby the expected insensitivity of the core radii to changes in the site symmetry and screening.

Figure 4 shows the contour plots of the components of the screening potential, as well as the total screening in the [110] plane in tungsten. Close to the atomic sites these potentials are spherical (as implied by the muffin-tin approximation), however nonspherical components are already noticeable at distances of the order of $\sim \frac{1}{2}a$ from the

atomic sites (whereas the muffin-tin sphere radius is of the order of $0.4a$)⁴⁰. Whereas the Coulomb screening assumes the form of a rounded rectangle around the atomic site [Fig. 4(a)], both the exchange and the correlation screening [Fig. 4(b) and 4(c), respectively] follow the general pattern of the charge density. The correlation screening is about an order of magnitude smaller than the exchange screening and varies very smoothly over most of the unit-cell space. Indeed, inclusion of $V_{\text{corr}}(\vec{r})$ into the one-body potential introduces an almost dispersionless downwards shift of the band structure $\epsilon_j(\vec{k})$ and only those band states which have appreciable magnitude near the core sites [where $V_{\text{corr}}(\vec{r})$ is nonuniform] are modified in a nonrigid manner.

The total screening field (Fig. 4d) is seen to be large near the nuclear site (where the Coulomb screening is large) and drops to smaller values in the interstitial regions (where the exchange-correlation screening is dominant). The absolute location of the zero line cannot be inferred from this calculation due to the omission of the zero momentum component of V_{Coul} . Note that the total screening potential points to the direction of the next-nearest neighbors, rather than the nearest neighbors. This introduces a higher gradient of the potential along the nearest-neighbor directions, producing larger forces along the bonds. The core pseudopotential is nearly spherical and hence the total effective potential carries basically the shape of the screening field.

B. Total energy

The band structure and total energy for Mo and W have been calculated at five values of the lattice constant $a/a_0 = 0.97, 0.99, 1.00, 1.01, \text{ and } 1.03$, where a_0 is the observed value (for Mo $a_0 = 3.15 \text{ \AA}$ and for W $a_0 = 3.16 \text{ \AA}$). Some typical values for the components of the total energy as well as the Fourier coefficients of the charge density in tungsten are given in Table III. Qualitatively similar trends are obtained for Mo. It is seen that the core-core energy (E_{Ewald}) and the $\vec{G} = 0$ component of the local core potential constitute the largest contribution to the total energy ($\sim 65\%$) while the rest of the terms are much smaller. The minimum in the total energy is obtained as a balance between the αZ_0 term (increasing with decreasing lattice constant) and the rest of the terms (decreasing with lowering the lattice constant). All the terms in E_{tot} behave monotonically with the lattice parameter and only E_{tot} shows an extremum. In particular, one notes that the sum of the energy eigenvalues does not form a measure to the total energy either in magnitude or in its lattice-parameter dependence.⁴⁶⁻⁴⁸

TABLE III. Variation in the components of the total energy of tungsten (sum of first seven terms in the table) with lattice parameter. Energies are given in Ry and the density Fourier components in e/cell , where $n(100)$ is normalized to 6.0. V_{scr} denotes the screening field $V_{\text{Coul}} + V_x + V_{\text{corr}}$. The primed sums indicate omission of the $\vec{G}=0$ term in V_{Coul} and V_{ps} .

Quantity	$a/a_0 = 0.97$	$a/a_0 = 1.00$	$a/a_0 = 1.03$
$\sum_{j,k} N_j(\vec{k}) \epsilon_j(\vec{k})$	-1.665 65	-1.376 59	-1.113 05
$-\sum_{\vec{G}} n(\vec{G}) V_{\text{scr}}(\vec{G})$	-0.261 10	-0.325 14	-0.416 586
$\frac{1}{2} \sum_{\vec{G}} n(\vec{G}) V_{\text{Coul}}(\vec{G})$	0.247 54	0.307 54	0.380 69
$-\frac{3}{4} \sum_{\vec{G}} n(\vec{G}) V_x(\vec{G})$	-3.617 70	-3.538 99	-3.461 15
αZ_v	12.282 88	11.211 24	10.260 221
E_{Ewald}	-22.617 94	-21.939 4	-21.300 39
$\sum_{\vec{G}} n(\vec{G}) \epsilon_c(\vec{G})$	-0.644 61	-0.638 73	-0.632 89
$\sum_{\vec{G}} n(\vec{G}) V_{\text{ps}}^{(l=0)}(\vec{G})$	0.127 92	0.740 97	0.973 97
E_{tot}	-16.276 58	-16.300 07	-16.283 157
$n(\bar{1}00)$	0.593 2	0.671 9	0.766 6
$n(1\bar{1}\bar{1})$	-0.072 5	-0.099 4	0.010 81
$n(20\bar{1})$	-0.051 5	-0.017 2	-0.015 9
$n(\bar{2}00)$	-0.077 3	-0.059 9	-0.068 3

This stems directly from the fact that the vacuum level to which the band eigenvalues should be referred, is by itself lattice-constant dependent due to the omission of the (volume dependent) individually divergent $\vec{G}=0$ terms from the Coulomb and pseudopotential terms in Eq. (2). We also note here that the volume variation of the pseudopotential band energies cannot be used to mimic pressure effects unless the volume dependence of the vacuum energy is explicitly calculated.

A large part of the lattice-constant variations of the screening energy was found to originate from the low momentum Fourier components of the charge density. These decrease rapidly with decreasing the lattice constant signaling an enhanced delocalization of the charge density as the d electrons interact more strongly.

The correlation energy is seen to be sizeable relative to the exchange energy. In the present calculation we have incorporated its effects in a self-consistent manner both in the one-body potential and in the total-energy expression. The correlation potential is hence allowed to modify the variational charge density, which in turn affects the noncorrelation contributions to the total energy. It is interesting to note that an *ad-hoc* non-self-consistent treatment of this term by sim-

ple addition of a Nozières-Pines⁴⁹ correlation term to the uncorrelated total energy produces relatively small errors, the difference between the latter and the self-consistently calculated correlation energy being -0.323 eV in Mo and -0.373 eV in tungsten. This is in line with the fact that in metallic systems the correlation potential is nearly constant over large portions of the unit cell (viz., Fig. 2) and introduces only very small additional dispersion in the energy bands. We note, however, that although the differences given above are relatively small on the scale of the cohesive energies of these materials (3%–5%), they are significantly large on the scale of the relevant structural-energy differences (e.g., fcc versus bcc).

We have previously indicated⁴ that the momentum and spatial variation of the correlation potential is rather different from that characteristic of the exchange potential and hence the former cannot be successfully reproduced by scaling the latter. At the same time we find that the correlation energy is approximately linearly correlated with the exchange energy over the entire range of lattice constants studied here. As the exchange and correlation energies E_x and E_{corr} appear in the total-energy expression as $\frac{3}{4}\alpha E_x + E_{\text{corr}}$ where α is the ex-

TABLE IV. Components of the total energy of tungsten and molybdenum at the calculated equilibrium lattice constant. 20 \vec{k} points are used to sample the BZ. $E_{\text{tot}}^{\text{atom}}$ denotes the spin-polarized atomic total pseudopotential energy. All quantities are given in Ry.

Quantity	Molybdenum	Tungsten
$\sum_{j,k} N_j(\vec{k})\epsilon_j(\vec{k})$	-0.728 19	-1.325 28
$-\sum_{\vec{G}}' n(\vec{G})V_{\text{scr}}(\vec{G})$	-0.692 55	-0.354 216
$\frac{1}{2}\sum_{\vec{G}}' n(\vec{G})V_{\text{Coul}}(\vec{G})$	0.611 17	0.320 706
$\frac{3}{4}\sum_{\vec{G}}' n(\vec{G})V_x(\vec{G})$	-3.646 66	-3.539 48
αZ_v	9.284 12	11.210 52
E_{Ewald}	-21.998 11	-21.939 40
$\sum_{\vec{G}} n(\vec{G})\epsilon_c(\vec{G})$	-0.644 33	-0.638 75
$E_{\text{tot}}^{\text{solid}}$	-17.814 55	-16.265 907
$E_{\text{tot}}^{\text{atom}}$	-17.323 51	-15.684 50
Binding energy	0.491	0.581

change scaling coefficient (for which we have presently adopted the value³ of $\alpha = \frac{2}{3}$ which yields the correct overall coefficient of $\frac{3}{4}\alpha = \frac{1}{2}$), one can attempt to mimic their combined effect by a $\frac{3}{4}\beta E_x$ term. This yields $\beta = 0.7870 \pm 0.0031$ for $0.97 \leq a/a_0 \leq 1.03$ in good agreement with the suggestion of Hedin and Lundquist⁵⁰ (for the electron density of W), $\alpha_{\text{eff}} = 0.77$.

The calculated total energies of Mo and W were fitted to a polynomial in the lattice-constant ratio a/a_0 . The equilibrium lattice parameter was found to be 3.152 Å for Mo (experimental value: 3.147 Å)⁵¹ and 3.173 Å for W (experimental value: 3.165 Å)⁵¹. At this calculated lattice constant, a total-energy calculation was repeated, using 20 \vec{k} points in the irreducible zone (rather than 14) for sampling the

wave functions. Table IV depicts the various components of the total energy for Mo and W. The individual contributions are seen to differ quite substantially in these materials, in particular the screening energies, the first-order repulsive term αZ_v and the eigenvalue sum.

As mentioned earlier, the most difficult convergence problem in the total-energy calculation arises here from the sampling of the charge density at various points in the Brillouin zone. From our results on the 20 \vec{k} -point sampling as well as from the other convergence tests, we infer an overall computational error of 0.02 Å in the lattice parameters and 0.002 Ry in the energies. Our calculation hence provides only a marginal distinction between the Mo and W lattice parameters.

The calculation of the cohesive energy poses an additional difficulty associated with the computation of the atomic total energy: The latter is not adequately described by the metallic exchange and correlation functionals used for the solid phases.^{52,53} A straightforward calculation of the ground-state spin-polarized (using the electron liquid exchange and correlation functional of Ref. 54) pseudopotential atomic total energies ($E_{\text{tot}}^{\text{atom}}$ in Table IV), however, produces a reasonable cohesive energy. The spin-polarization energies obtained here for the pseudoatoms (-4.5,⁵⁵ and -3.50 eV for Mo and W, respectively) are large on the scale of the binding energies and cannot be neglected.

Table V summarizes the calculated and measured^{51,56,57} bulk properties of Mo and W. As the zero-point energy is rather small in these systems (0.003 Ry) we did not apply this correction to the calculated quantities. Our calculated values for the equilibrium lattice constant, cohesive energy and bulk modulus are within 0.25%, 11%, and 12% of the experimental values, respectively. Hence the cohesive energy calculation involves the uncertainties associated with the atomic energy, the disagreement between the computed and experimental cohesive energies should not be taken

TABLE V. Calculated and observed bulk properties of Mo and W. A_{eq} , BE, and B denote, respectively, lattice parameter, binding energy, and bulk modulus.

Quantity	Molybdenum	Tungsten
$A_{\text{eq}}^{\text{calc}}$ (Å)	3.152	3.173
$A_{\text{eq}}^{\text{expt}}$ (Å)	3.147 (Ref. 51)	3.165 (Ref. 51)
BE ^{calc} (eV)	6.68	7.90
BE ^{expt} (eV)	6.82	8.90 (Ref. 56)
B^{calc} (dyn/cm ²)	3.05×10^{12}	3.45×10^{12}
B^{expt} (dyn/cm ²)	2.725×10^{12} (Ref. 52)	3.232×10^{12} (Ref. 52)

strictly as characteristic of the accuracy of the other bulk properties. The bulk properties of W were not calculated before, however Moruzzi, Janak, and Williams⁵⁸ have performed a self-consistent muffin-tin calculation of the bulk properties of Mo. Their results for the lattice constant, cohesive energy, and bulk modulus are 3.12 Å, 6.73 eV, and 2.5×10^{12} dyn/cm², respectively, in good agreement (deviations of 1%, 0.7%, and 18%, respectively) with the results of the present study. Whereas the calculated equilibrium lattice parameters of Mo and W are of comparable accuracy, our calculated cohesive energy for W is in substantially poorer agreement with experiment than the corresponding results for Mo. Since the present calculation neglects completely relativistic effects, it is impossible to identify the microscopic origin of this trend. Our calculated values for the bulk moduli over estimate the observed values for Mo and W by 12% and 7%, respectively. Other calculated values for transition and nontransition metals^{23,24,58} indicate similar over estimation.

V. SUMMARY AND CONCLUSIONS

We have used an efficient method for computing the total pseudopotential crystal energy in a momentum-space representation. The method avoids any shape approximation to the variational charge density (e.g., muffin-tin), is fully self-consistent and replaces all the multidimensional and multi-center integrations characteristic of the real-space representations by simple single summations in momentum space. The convergence characteristics of this method have been carefully examined for two transition metals. This poses a stringent test on the accuracy of the method as these systems are characterized by highly localized states with pronounced pseudopotential nonlocality. A mixed basis representation for the crystalline wave function was shown to be sufficiently flexible to overcome all the momentum-space convergence difficulties to within a few mRy accuracy. The pseudopotentials used in this work do not involve any fitting to band structure or atomic term value data. In turn, they are obtained by a direct inversion of the density-functional all-electron atomic eigenvalue problem. The excellent agreement obtained here with the observed bulk properties of Mo and W together with the previously established quality of the band structure and charge density of transition metals^{4,5} and semiconductors,¹ provide strong support for the quality of these first-principles pseudopotentials.

The present work has completely neglected relativistic effects on the total energy and bulk properties. The larger errors involved in the W binding energy might be indicative of this approximation.

The underlying approximation of the present pseudopotential approach is the assumption of a frozen core. In developing the core pseudopotential,^{1,2} we assume that the dynamic effect of the core electrons on the valence field can be replaced by a static potential derived from the atomic ground-state core wave functions. As a result, we are able to transform the all-electron problem with its associated large total energy (e.g., -30,551 Ry for W of which the observed cohesive energy forms only 0.002%) to a much simpler pseudopotential problem having a small valence total energy (e.g., -16.3 Ry in W, of which the cohesive energy forms 4%). Although this increase of the ratio between the cohesive energy and the total energy by three orders of magnitude constitutes an attractive feature of this approach (particularly for application to complex many-electron systems such as surfaces and transition-metal compounds), the frozen-core approximation should be treated with care. A recent KKR (Korringa-Kohn-Rostoker) study⁵⁹ on Mo has indicated that whereas all core eigenvalues increase by an approximately constant amount of 0.25 eV/electron when the crystal phase changes from fcc to bcc, the 4*p* core kinetic energy shifts by 0.36 eV/electron while all other core kinetic energies are approximately unchanged. This change of phase is similarly accompanied by small energy lowering in the valence 5*s* and 5*p* states while the 4*d* state stabilizes by as much as 1.18 eV. In the pseudopotential formalism all the structurally induced energetic changes are restricted to the valence states. The present study on Mo and W indicates that the changes in the core and valence states in going from the atom to the solid are successfully reproduced by the dynamic response of the valence states alone in the presence of a ground-state static core potential. As the core orthogonality constraint is lifted in the pseudopotential representation, the valence states are redistributed in the solid in a different manner than in the all-electron representation, leading in the present case to substantial modifications in the 4*d* as well as in the 5*s* and 5*p* orbital and kinetic energies. Clearly, however, as the "united atom" limit does not exist in the pseudopotential model, one expects that the replacement of the effects of the core electrons by a ground state derived static potential will fail at sufficiently small interatomic distances. At present, it is difficult to assess the extent of the structurally induced core perturbations which will invalidate the pseudopotential representation.

ACKNOWLEDGMENTS

This work was supported in part by the Division of Basic Energy Sciences, U. S. Department of

Energy, and by NSF Grant No. DMR76-20647-A01. The authors are grateful to A. R. Williams for helpful discussions and for making his results on the Mo total energy available prior to their publication.

APPENDIX A

The plane wave representation Eqs. (14)–(18) of the mixed basis wave function makes the evaluation of the Hamiltonian matrix element simple.¹¹ If $\Phi_{\mu\alpha}(\vec{k}, \vec{r})$ denotes an LCAO type Bloch function [Eq. (16)] and $|\vec{k} + \vec{G}\rangle$ denotes a plane-wave Bloch function, the elements are as follows:

(i) overlap:

$$\langle \Phi_{\mu\alpha}(\vec{k}, \vec{r}) | \Phi_{\nu\beta}(\vec{k}, \vec{r}) \rangle = \sum_{\vec{G}} T_{\alpha}(\vec{G}) T_{\beta}(\vec{G}) \times d_{\mu\alpha}(\vec{k} + \vec{G}) d_{\nu\beta}(\vec{k} + \vec{G}), \quad (\text{A1})$$

$$\langle \Phi_{\mu\alpha}(\vec{k}, \vec{r}) | \vec{k} + \vec{G} \rangle = T_{\alpha}(\vec{G}) d_{\mu\alpha}(\vec{k} + \vec{G}), \quad (\text{A2})$$

$$\langle \vec{k} + \vec{G} | \vec{k} + \vec{G}' \rangle = \delta_{\vec{G}\vec{G}'}, \quad (\text{A3})$$

where $T_{\alpha}(\vec{G})$ and $d_{\mu\alpha}(\vec{k} + \vec{G})$ are given by Eq. (17) and the (analytical) Fourier transform of Eq. (15).

(ii) kinetic:

$$\langle \Phi_{\mu\alpha}(\vec{k}, \vec{r}) | -\frac{1}{2}\nabla^2 | \Phi_{\nu\beta}(\vec{k}, \vec{r}) \rangle = \sum_{\vec{G}} T_{\alpha}(\vec{G}) T_{\beta}(\vec{G}) d_{\mu\alpha}(\vec{k} + \vec{G}) d_{\nu\beta}(\vec{k} + \vec{G}) (\vec{k} + \vec{G})^2, \quad (\text{A4})$$

$$\langle \Phi_{\mu\alpha}(\vec{k}, \vec{r}) | -\frac{1}{2}\nabla^2 | \vec{k} + \vec{G} \rangle = T_{\alpha}(\vec{G}) d_{\mu\alpha}(\vec{k} + \vec{G}) (\vec{k} + \vec{G})^2, \quad (\text{A5})$$

$$\langle \vec{k} + \vec{G} | \vec{k} + \vec{G}' \rangle = (\vec{k} + \vec{G})^2 \delta_{\vec{G}\vec{G}'}. \quad (\text{A6})$$

(iii) potential: If $W_{L,NL}$ denotes the total screened potential

$$W_{L,NL} = V_{L,NL} + V_{\text{Coul}} + V_x + V_{\text{corr}}, \quad (\text{A7})$$

where $V_{L,NL}$ denotes either the local (L) or the nonlocal (NL) pseudopotential, the matrix elements are given as

$$\langle \Phi_{\mu\alpha}(\vec{k}, \vec{r}) | W | \Phi_{\nu\beta}(\vec{k}, \vec{r}) \rangle = \sum_{\vec{G}} \sum_{\vec{G}'} T_{\alpha}(\vec{G}) T_{\beta}(\vec{G}') d_{\mu\alpha}(\vec{k} + \vec{G}) d_{\nu\beta}(\vec{k} + \vec{G}') \times \langle \vec{k} + \vec{G} | W | \vec{k} + \vec{G}' \rangle, \quad (\text{A8})$$

where

$$\langle \vec{k} + \vec{G} | W | \vec{k} + \vec{G}' \rangle = \langle \vec{k} + \vec{G} | V_L + V_{\text{Coul}} + V_x + V_{\text{corr}} \times |\vec{k} + \vec{G}'\rangle \delta_{\vec{G}\vec{G}'} + \langle \vec{k} + \vec{G} | V_{NL} | \vec{k} + \vec{G}' \rangle. \quad (\text{A9})$$

Hence for the local component the double sum in Eq. (A8) reduces to a single sum. This requires the knowledge of the screened local potential in momentum space

$$V_{\text{eff},L}(\vec{Q}) = V_L(\vec{Q}) + V_{\text{Coul}}(\vec{Q}) + V_x(\vec{Q}) + V_{\text{corr}}(\vec{Q}). \quad (\text{A10})$$

The first term is calculated by a one-dimensional radial integration of the single-site potential $U_L(r)$ [Eq. (12)] combined with a structure factor: $V_L(Q) = U_L(Q)S(Q)$ whereas the rest of the terms in Eq. (A10) are calculated as indicated in the text [Eqs. (20)–(22)]. The off-diagonal element $\langle \vec{k} + \vec{G} | V_{NL} | \vec{k} + \vec{G}' \rangle$ is calculated by decomposing the plane waves into spherical Bessel functions and Legendre polynomials $P_l(\cos\theta_{\vec{G}\vec{G}'})$ and operating on the latter with the angular-momentum projection operator P_l [Eq. (12)],

$$\langle \vec{k} + \vec{G} | V_{NL} | \vec{k} + \vec{G}' \rangle = \frac{4\pi}{\Omega} \sum_{\alpha} S_{\alpha}(\vec{G} - \vec{G}') \sum_{l=1}^{\infty} (2l+1) \times P_l(\cos\theta_{\vec{G}\vec{G}'}) F_l(\vec{k} + \vec{G}, \vec{k} + \vec{G}'), \quad (\text{A11})$$

where

$$F_l(\vec{Q}, \vec{Q}') = \langle j_l(|\vec{Q} \cdot \vec{r}|) | U_l(\vec{r}) - U_L^{(l)} | j_l(|\vec{Q}' \cdot \vec{r}|) \rangle. \quad (\text{A12})$$

Here $j_l(Qr)$ denotes the spherical Bessel function and $U_l(\vec{r})$ and $U_L(\vec{r})$ are the atomic nonlocal and local ($l=0$) pseudopotentials [Eqs. (6) and (12)]. The elements $F_l(Q, Q')$ are calculated by one-dimensional numerical integration.

The matrix element of W within the localized-plane-wave states are

$$\langle \Phi_{\mu\alpha}(\vec{k}, \vec{r}) | W | \vec{k} + \vec{G} \rangle = \sum_{\vec{G}'} T_{\alpha}(\vec{G}') d_{\mu\alpha}(\vec{k} + \vec{G}') \times \langle \vec{k} + \vec{G}' | W | \vec{k} + \vec{G}' \rangle, \quad (\text{A13})$$

whereas the plane-wave–plane-wave elements are simply

$$\langle \vec{k} + \vec{G} | W | \vec{k} + \vec{G}' \rangle.$$

If we denote by $\vec{G}_{\text{max}}^{(3)}$ the largest momentum appearing in the crystal wave function [cf. Eq. (18)], a fully converged representation of the Hamiltonian matrix requires a maximal cut-off of $|\vec{G}_{\text{max}}^{(3)} - \vec{G}'_{\text{max}}^{(3)}| \leq 2|\vec{G}_{\text{max}}^{(3)}|$. In practice, however, somewhat smaller cutoff momenta ($\approx 1.5|\vec{G}_{\text{max}}^{(3)}|$) are usually sufficient to obtain well converged (~ 0.03 eV) energy eigenvalues.

- *Present address: Solar Energy Research Institute, Golden, Colo. 80401.
- ¹A. Zunger and M. L. Cohen, Phys. Rev. B (to be published).
 - ²A. Zunger and M. Ratner, Chem. Phys. **30**, 423 (1978).
 - ³W. Kohn and L. J. Sham, Phys. Rev. **140**, A 1133 (1965).
 - ⁴A. Zunger and M. L. Cohen, Phys. Rev. B (to be published).
 - ⁵A. Zunger, G. P. Kerker, and M. L. Cohen (unpublished).
 - ⁶(a) A. Zunger and M. L. Cohen, Phys. Rev. Lett. **41**, 53 (1978); (b) J. R. Chelikowsky and J. C. Phillips, Phys. Rev. B **17**, 2453 (1978); (c) J. St. John and A. N. Bloch, Phys. Rev. Lett. **33**, 1095 (1974).
 - ⁷J. Ihm, A. Zunger, and M. L. Cohen (unpublished).
 - ⁸G. G. Wepfer, R. N. Euwema, G. T. Surratt, and D. L. Willhite, Phys. Rev. B **9**, 2670 (1974).
 - ⁹R. N. Euwema and R. L. Green, J. Chem. Phys. **62**, 4455 (1975).
 - ¹⁰A. Zunger and A. J. Freeman, Phys. Rev. B **15**, 4716 (1977); **15**, 5049 (1977); **16**, 2901 (1977).
 - ¹¹S. G. Louie, K. M. Ho, and M. L. Cohen (unpublished).
 - ¹²R. N. Euwema, Phys. Rev. B **4**, 4332 (1971).
 - ¹³R. N. Euwema, Int. J. Quantum Chem. **5**, 61 (1971).
 - ¹⁴R. A. Deegan and W. D. Twose, Phys. Rev. **164**, 993 (1967).
 - ¹⁵A. B. Kunz, J. Phys. C **3**, 1542 (1970).
 - ¹⁶N. O. Lipari and A. B. Kunz, Phys. Rev. B **2**, 491 (1970).
 - ¹⁷K. S. Singwi, A. Sjölander, P. M. Tosi, and R. H. Land, Phys. Rev. B **1**, 1044 (1970).
 - ¹⁸J. C. Phillips and L. Kleinman, Phys. Rev. **116**, 287 (1959).
 - ¹⁹M. L. Cohen and V. Heine, in *Solid State Physics*, edited by H. Ehrenreich, F. Seitz, and D. Turnbull (Academic, New York, 1970), Vol. 24, p. 38; D. Brust, in *Methods in Computational Physics*, edited by B. Alder, S. Fernbach, and M. Rotenberg (Academic, New York, 1968), Vol. 8, p. 33.
 - ²⁰N. W. Ashcroft, Phys. Lett. **23**, 48 (1966); N. W. Ashcroft and D. C. Langreth, Phys. Rev. **155**, 682 (1967); **159**, 500 (1967).
 - ²¹I. V. Abarenkov and V. Heine, Philos. Mag. **12**, 529 (1965); V. Heine and I. V. Abarenkov, *ibid.* **9**, 451 (1963).
 - ²²P. D. DeCicco, Ph.D. thesis (Massachusetts Institute of Technology, September 1965) (unpublished).
 - ²³F. W. Averill, Phys. Rev. B **6**, 3637 (1972).
 - ²⁴E. C. Snow, Phys. Rev. B **8**, 5391 (1973).
 - ²⁵J. F. Janak, Phys. Rev. B **9**, 3985 (1974).
 - ²⁶G. S. Painter, D. E. Ellis, and A. R. Lubinsky, Phys. Rev. B **4**, 3610 (1971); A. R. Lubinsky, D. E. Ellis, and G. S. Painter, *ibid.* **11**, 1537 (1975).
 - ²⁷J. B. Danese, J. Chem. Phys. **61**, 3071 (1974); J. B. Danese and J. W. D. Connolly, Int. J. Quantum Chem. **S7**, 279 (1973).
 - ²⁸A. Zunger and A. J. Freeman, Phys. Rev. B **16**, 906 (1977).
 - ²⁹F. E. Harris and H. J. Monkhorst, Solid State Commun. **9**, 1449 (1971).
 - ³⁰W. Y. Ching and J. Callaway, Phys. Rev. B **9**, 5115 (1974).
 - ³¹A. Zunger and A. J. Freeman, Int. J. Quantum Chem. **S11**, 539 (1977).
 - ³²R. A. Coldwell-Horsfall and A. A. Maradudin, J. Math. Phys. **1**, 395 (1960).
 - ³³W. A. Harrison, in *Pseudopotentials in the Theory of Metals* (Benjamin, New York, 1966).
 - ³⁴D. Weaire, Phys. Status Solidi **42**, 767 (1970).
 - ³⁵J. A. Moriarty, Phys. Rev. B **16**, 2537 (1977); **10**, 3075 (1974).
 - ³⁶J. W. Cooley and J. W. Tukey, Math. Computation **19**, 297 (1965).
 - ³⁷D. J. Chadi and M. L. Cohen, Phys. Rev. B **8**, 5747 (1973).
 - ³⁸G. Lehman and M. Taut, Phys. Status Solidi **54**, 469 (1971).
 - ³⁹P. O. Löwdin, Int. J. Quantum Chem. **S1**, 811 (1967).
 - ⁴⁰L. F. Mattheiss, Phys. Rev. **134**, 970 (1964); **139**, 1893 (1965).
 - ⁴¹S. L. Altmann and C. J. Bradley, Proc. Phys. Soc. London **92**, 764 (1967).
 - ⁴²H. Wendel and R. M. Martin, Phys. Rev. Lett. **40**, 950 (1978).
 - ⁴³J. F. Alward, C. Guha Sridhar, C. M. Perlov, and C. Y. Fong, Phys. Rev. B **15**, 5724 (1977).
 - ⁴⁴C. Y. Fong and M. L. Cohen, Phys. Rev. Lett. **24**, 306 (1970).
 - ⁴⁵G. P. Kerker, K. M. Ho, and M. L. Cohen (unpublished).
 - ⁴⁶D. J. Chadi and R. M. Martin, Solid State Commun. **19**, 643 (1976).
 - ⁴⁷K. Rudenberg, J. Chem. Phys. **66**, 375 (1977).
 - ⁴⁸N. H. March, J. Chem. Phys. **67**, 4618 (1977).
 - ⁴⁹P. Nozières and D. Pines, Phys. Rev. **111**, 442 (1958).
 - ⁵⁰L. Hedin and B. I. Lindqvist, J. Phys. C **4**, 2064 (1971).
 - ⁵¹R. W. G. Wyckoff, in *Crystal Structure* (Wiley, New York, 1963), Vol. 1, p. 19.
 - ⁵²B. Y. Tong and L. J. Sham, Phys. Rev. **144**, 1 (1966).
 - ⁵³B. Y. Tong, Phys. Rev. A **4**, 1375 (1971).
 - ⁵⁴U. von Barth and L. Hedin, J. Phys. C **5**, 1629 (1972).
 - ⁵⁵The value of -4.15 eV obtained here for the Mo pseudo atom is close to that obtained by A. R. Williams (private communication) for the real atom (-4.4 eV), in accord with the fact that the valence pseudoorbitals reproduce very accurately the all-electron wave functions in the tail region.
 - ⁵⁶C. Kittel, in *Introduction to Solid State Physics*, 5th ed. (Wiley, New York, 1976), p. 74.
 - ⁵⁷C. Kittel, see Ref. 56, p. 85.
 - ⁵⁸J. F. Janak, V. L. Moruzzi, and A. R. Williams, Phys. Rev. B **12**, 1257 (1975).
 - ⁵⁹A. R. Williams (private communication).